




Novel alginate biphasic scaffold for osteochondral regeneration: an in vivo evaluation in rabbit and sheep models

Giuseppe Filardo¹ · Francesco Perdisa¹  · Michael Gelinsky² · Florian Despong² · Milena Fini^{3,4} · Maurilio Marcacci^{5,6} · Anna Paola Parrilli³ · Alice Roffi¹ · Francesca Salamanna³ · Maria Sartori³ · Kathleen Schütz² · Elizaveta Kon^{5,6}

Received: 29 August 2017 / Accepted: 21 April 2018 / Published online: 26 May 2018
© Springer Science+Business Media, LLC, part of Springer Nature 2018

Abstract

Current therapeutic strategies for osteochondral restoration showed a limited regenerative potential. In fact, to promote the growth of articular cartilage and subchondral bone is a real challenge, due to the different functional and anatomical properties. To this purpose, alginate is a promising biomaterial for a scaffold-based approach, claiming optimal biocompatibility and good chondrogenic potential. A previously developed mineralized alginate scaffold was investigated in terms of the ability to support osteochondral regeneration both in a large and medium size animal model. The results were evaluated macroscopically and by microtomography, histology, histomorphometry, and immunohistochemical analysis. No evidence of adverse or inflammatory reactions was observed in both models, but limited subchondral bone formation was present, together with a slow scaffold resorption time.

The implantation of this biphasic alginate scaffold provided partial osteochondral regeneration in the animal model. Further studies are needed to evaluate possible improvement in terms of osteochondral tissue regeneration for this biomaterial.

1 Introduction

The treatment of articular surface defects remains a challenge in orthopaedic surgery, since the osteochondral unit has a very low regenerative potential, and no treatment has yet demonstrated the ability to provide repair tissues with properties comparable to the healthy native ones [1, 2]. Whereas most of the attention was paid to the cartilaginous layer in the past, increasing evidence shows the close correlation of articular cartilage with the status underlying subchondral bone, which is involved in the pathogenetic process and may affect treatment results [3]. The restoration of both cartilage and bone is emerging as a key aspect to properly restore the osteochondral unit, but presents challenges related with the need to address two tissues with different structure and properties. Recently, the use of biomaterials able to enhance the in situ osteochondral regeneration has been introduced with positive findings in the animal model [4], but only very few of these constructs have been tested in the clinical practice [5, 6] with controversial results. The first scaffold reported for clinical use, a polylactide-coglycolide copolymer, showed poor repair

✉ Francesco Perdisa
dr.perdisa@gmail.com

¹ Nano-Biotechnology (NABI) Laboratory, Rizzoli RIT Department, Rizzoli Orthopaedic Institute, Via di Barbiano 1/10, Bologna 40136, Italy

² Centre for Translational Bone, Joint and Soft Tissue Research, University Hospital and Faculty of Medicine, Technische Universität Dresden, Fetscherstr. 73, Dresden 01307, Germany

³ Laboratory of Biocompatibility, Innovative Technologies and Advanced Therapies, Rizzoli RIT Department, Rizzoli Orthopaedic Institute, Via di Barbiano 1/10, Bologna 40136, Italy

⁴ Laboratory of Preclinical and Surgical Studies, Rizzoli Orthopaedic Institute, Via di Barbiano 1/10, Bologna 40136, Italy

⁵ Knee Joint Reconstruction Center - 3rd Orthopaedic Division, Humanitas Clinical Institute, Via Alessandro Manzoni 56, Rozzano, Milan, Italy

⁶ Department of Biomedical Sciences, Humanitas University, Via Manzoni 113, Rozzano, Milan, Italy

tissue quality at imaging, as well as unsatisfactory clinical outcomes [1]. The second osteochondral scaffold, a biomimetic nanostructured construct, organized in different layers of type I collagen and hydroxyapatite (HA) [7], was developed to better mimic structure and composition of the whole osteochondral unit, showing promising clinical results even in challenging conditions, such as complex lesions or osteoarthritic knees [8, 9]. However, imaging evaluation showed a limited osteochondral regeneration potential, with a slow tissue regeneration progression, and significant abnormalities persisting over time [10]. Other materials, conceived with different rationale, gave promising preliminary results, but have not reached the clinical practice, yet. Thus, the regeneration of the osteochondral unit remains an unmet clinical need, which claims for further investigations in order to obtain biomaterials with better properties able to improve the overall regeneration potential.

Alginate is a natural polysaccharide derived from marine algae. It has previously been demonstrated that it presents a good potential for engineering cartilage tissue *in vitro*, since it supports the maintenance of rounded morphology and phenotype of chondrocytes [11–14]. Moreover, alginate is dimensionally stable, and it is expected to support chondrogenic differentiation due to the absence of adhesive domains that may inhibit chondrogenesis [15]. In fact, chondrocytes within alginate gels were reported to remain viable and maintain their phenotype [11, 16]. Furthermore, Diduch et al. [17] found that embedding hMSC into an alginate gel can be chondroinductive.

Alginate is a natural-derived polymer that can undergo to gentle gelation with multivalent cations like Ca^{2+} in order to obtain hydrogels, and alginate-derived hydrogels showed excellent compatibility with biological components, including growth factors (GFs) and cells [18]. They represent promising candidates for bioengineered materials, also as suitable options for the development of treatments targeted to osteochondral defects [19]. Thus, a biphasic alginate-based scaffold was developed by assembling alginate and HA for the bone layer, whereas alginate was combined with hyaluronic acid (HYA) for the chondral phase [20].

Aim of this study was to investigate the osteochondral regenerative potential of this alginate-based biphasic scaffold *in vivo*, by conducting a pilot study on a large-size clinically relevant model to evaluate its performance in terms of osteochondral unit restoration. Furthermore, a medium-size animal model (rabbit) was used to specifically analyze the ability of mineralized alginate-HA to regenerate bone tissue and understand its contribution to the overall results in terms of osteochondral regeneration.

2 Materials and methods

2.1 Scaffold preparation

Biphasic alginate-based scaffolds were fabricated according to the principle of diffusion controlled, directed ionotropic gelation of alginate, leading to the formation of parallel aligned channel-like pores through the whole length of the scaffolds as previously described by Schütz et al. [20]. In brief, the bony layer consisted of a composite made of 1.25% alginate and 4% HA, the chondral layer of 1% alginate and 0.5% HYA. An additional low percentage (0.5%) alginate layer was added on top, serving as a sacrificial layer in order to protect the underlying chondral one. The different layers were fused together during alginate gelation with calcium ions, thus leading to the formation of biphasic but monolithic scaffolds. The complete procedure was carried out under sterile conditions. After completed gelation, the sacrificial layer was cut and cylinders of 7 mm diameter and 5 mm depth could be punched for the sheep study (1 mm chondral and 4 mm bone layer). For the rabbit animal study, only the bony-like layer was used for the scaffold production and implantation.

2.2 Surgical procedures

The *in vivo* study was performed complying with the European and National Law on animal experiments, after the approval of the research protocol by the Local Ethical Committee. All the animals were purchased from authorized farms and submitted to a quarantine period before their utilization.

2.2.1 Sheep model

Six crossbred adult sheep, 65 ± 5 kg b.w. (Breeder: Pancaldi Raffaele, Bologna, Italy), were housed in standard and controlled conditions (22 ± 1 °C, $50 \pm 5\%$ RH, ventilation of 10 air changes per hour). The animals were divided into 2 groups according to the treatment.

Group 1 ($n = 2$, control): untreated;

Group 2 ($n = 4$, experimental): biphasic HA-HYA alginate scaffold.

Surgery was conducted under general anesthesia and assisted ventilation. A median longitudinal skin incision and parapatellar approaches to the joint were performed, in order to expose the medial and lateral condyle. A critical size osteochondral defect (diameter: 7 mm, depth: 5 mm) was prepared in the weight-bearing region of medial and

lateral femoral condyles using a drill specifically designed to obtain reproducible standardized lesions. Osteochondral grafts were implanted into the defects using press-fit fixation and wound was then sutured. Standard antibiotic and analgesic therapy was administered i.m. in the postoperative period. All animals were euthanized 6 months after surgery by injection of Tanax® (Intervet-Italia S.r.l., Milan, Italy) under general anesthesia.

2.2.2 Rabbit model

Twelve adult male New Zealand rabbits (Harlan Laboratories SRL, S. Pietro al Natissone, Udine), were housed in standard and controlled conditions (22 ± 1 °C, $55 \pm 5\%$ RH) and fed with a standard diet (Mucedola, Milano, Italy) and water ad libitum. Surgery was carried out under general anesthesia and assisted ventilation. The distal femoral epiphysis was exposed through a 2 cm longitudinal skin incision, then cylindrical critical size defects (diameter: 6 mm, length: 8 mm) were created bilaterally in the femoral epiphysis by using a drill.

Scaffolds were implanted as follows:

Group 1 ($n = 6$, control): commercially available collagen-hydroxyapatite composite scaffold (Rege-noss™, Finceramica s.p.a., Faenza, Italy);

Group 2 ($n = 6$, experimental): mineralized HA-alginate scaffold.

After wound suture, all animals underwent standard antibiotics and analgesics administration. At planned time (2 days on—10 days off—2 days on) before the 8 weeks of experimental time, animals received an i.m. injection of oxytetracycline (30 mg/kg) to assess bone tissue growth through dynamic histomorphometry. Sacrifices were performed with i.v. administration of Tanax® (Hoechst AG, Frankfurt am Main, Germany) under anesthesia.

2.3 Samples evaluation

2.3.1 Macroscopic evaluation

Femoral condyles were excised, stripped of soft tissues, and underwent macroscopic evaluation.

Each sample was evaluated for any signs of inflammation or adhesions. The macroscopic appearance of the sheep implants and the quality of healing were blindly assessed using the Fortier modified scoring system [21]. A gross morphological evaluation using a scoring system proposed by Niederauer was also performed [22]. Finally, each sample was cut in half along the central axis of the implant and evaluated by microtomography, histology and immunohistochemistry.

2.3.2 Microtomography

Samples were scanned with the high resolution microtomography Skyscan 1176 (Bruker Micro-CT, Belgium) at a voltage of 50 kV, current of 500 μ A and using an aluminum filter of 0.5 mm.

Each sample was rotated by 180° with a rotation step of 0.4° according to the following set up: rabbit, average frame of 2, nominal resolution 9- μ m; sheep, average frame of 3, nominal resolution 17.5 μ m. The acquired images were reconstructed by the NRecon software (1.6.8.0) with corrections for alignment beam hardening and ring artefact reduction, and 3D models were created to allow visualizations of the samples in space (Fig. 1).

Two specific Volume of Interest (VOIs) were defined in each sample. TV₁: cylindrical VOI with diameter of 6-mm and height of 8-mm or diameter of 7-mm and height 5-mm for rabbits and sheep, respectively, and used to evaluate the material and the new bone formation into the defect. TV₂: VOI of the trabecular bone of the condyle in the area around the defect with the same height of TV₁ (used to evaluate peri-implant bone) (Fig. 2). Then, morphological parameters were calculated:

1. Defect BV/TV₁ (%), ratio between the volume of newly formed bone within the bone defect and the total volume of the bone defect;
2. Defect Trabecular Thickness (Tb.Th, mm), calculated in a model independent way [23] over the total volume of the bone defect TV₁;
3. Defect Trabecular Number (Tb.N, mm⁻¹), the number of intersections through a trabecular structure per unit length of a random linear path through TV₁;
4. Defect Trabecular Separation (Tb.Sp, mm), calculated as the Tb.Th;
5. Peri-implant BV/TV₂ (%), ratio between the volume of trabecular bone around the bone defect and the total volume of interest TV₂;
6. Peri-implant Tb.Th Trabecular Thickness, Tb.N Trabecular Number and Tb.Sp Trabecular Separation calculated as above (in TV₂).

2.3.3 Histology and histomorphometry

Sheep—Each sample was cut in half along the central axis of the implant. Half was directly processed for resin embedding; half was decalcified and embedded in paraffin. The latter samples were fixed in 10% formalin and decalcified in a nitric/formic acid solution for about 2 weeks. When decalcification was complete, the samples were dehydrated in a graded series of alcohol from 70% to absolute and then processed for paraffin embedding. Five-micrometer-thick sections were obtained by a Microm

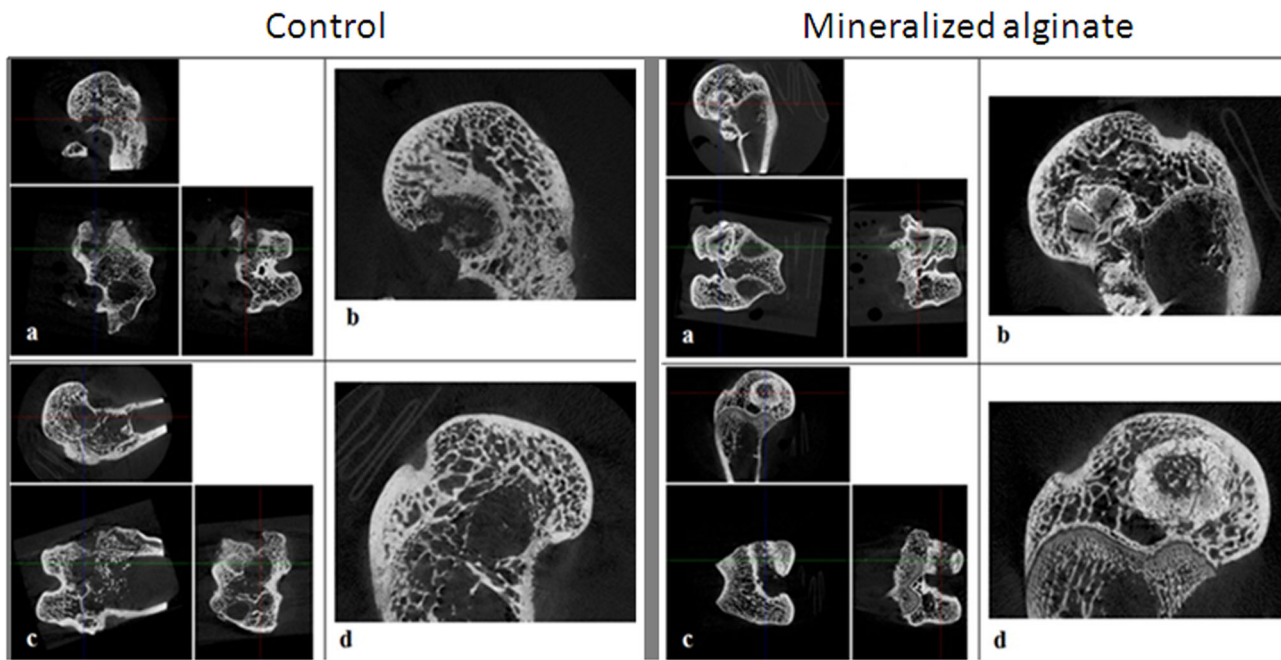


Fig. 1 Micro-CT sections of control (RegenOss) (left panel) and experimental group (right panel), in the rabbit model. Each panel is organized as follows: **a** Micro-CT sections in the three spatial planes (axial, sagittal and coronal) of the right leg samples; **b** Sagittal micro-CT section of the lateral condyle of the right leg samples; **c** Micro-CT sections in the three spatial planes (axial, sagittal and coronal) of the

left leg samples; **d** Sagittal micro-CT section of the lateral condyle of the left leg samples. Control group showed little new bone growth inside the defect and a thin trabecular new bone structure, whereas the material was still partially present in the experimental group, with new bone growth both inside and around the implant and a good level of osteointegration

HM340E (Microm International GmbH, Germany) and stained with hematoxylin/eosin.

The specimens of undecalcified bone processing histology were first fixed in 4% paraformaldehyde, dehydrated in graded series of alcohol and then embedded in polymethylmetacrylate (Merck, Schuchardt, Germany). Blocks were sectioned along a plane parallel to the long axis of the osteochondral transplant. Sections were then grounded up to a thickness of $40 \pm 10 \mu\text{m}$ (Saphir apparatus 550, ATM GmbH, Germany), stained with Safranin-O/Fast Green.

The decalcified and undecalcified sections were processed for histological analysis and grabbed at $20\times$ magnification using the light Olympus BX51 microscope (BX51, Olympus Optical Co. Europe GmbH, Germany) connected to the XC50 Olympus digital camera (Olympus Optical Co. Europe GmbH, Germany). Comparative semiquantitative analysis was performed using the Pineda scale [24].

Rabbits—The femoral distal epiphyses were undecalcified and fixed in 4% paraformaldehyde, dehydrated in a graded series of alcohol and finally embedded in polymethylmetacrylate (Merck, Schuchardt, Hohenbrunn, Germany). Blocks were sectioned perpendicular to the bone surface using a diamond saw microtome into sections $100 \pm 10 \mu\text{m}$ thick, then they were grounded to a thickness of $15 \pm 5 \mu\text{m}$ (Saphir apparatus 550, ATM GmbH, Germany). Three sections for each sample were stained with Stevenel Blue/Van Gieson Picrofuchsin for the histological investigations,

whereas other three were left unstained for oxytetracycline incorporation assay [25].

Regarding oxytetracycline incorporation, 5 regions of interest (ROI) around or into the scaffolds were grabbed at $20\times$ magnification using a light/fluorescence microscope connected to a digital camera and to an image analysis software (BX51, Olympus Optical Co. Europe GmbH, Germany). Mineral Apposition Rate (MAR, $\mu\text{m}/\text{day}$) and Bone Formation Rate (BFR/B.Pm $\mu\text{m}^2/\mu\text{m}/\text{day}$) were assessed by applying the nomenclature and methodology of the American Society of Bone and Mineral Research (ASBMR) [26].

2.3.4 Immunohistochemical analysis

Sheep—Two sections of decalcified and paraffin-embedded samples were immunostained for Collagen I, Collagen II and Vascular Endothelial Growth Factor (VEGF). Briefly, after fixation, sections were extensively rinsed in PBS and permeabilized by incubation in 0.3% hydrogen peroxide in PBS solution. Sections to be immunostained were pre-treated for antigen unmasking with 0.2% Pronase (Sigma, Mo, USA) solution in PBS. Subsequently, 10% normal serum was added to block nonspecific antibody binding, and the primary antibodies (Thermo Fisher Scientific Inc, USA) were applied. After rinsing in PBS, slides were incubated with appropriate biotinylated secondary antibody and with horseradish peroxidase-streptavidin complex

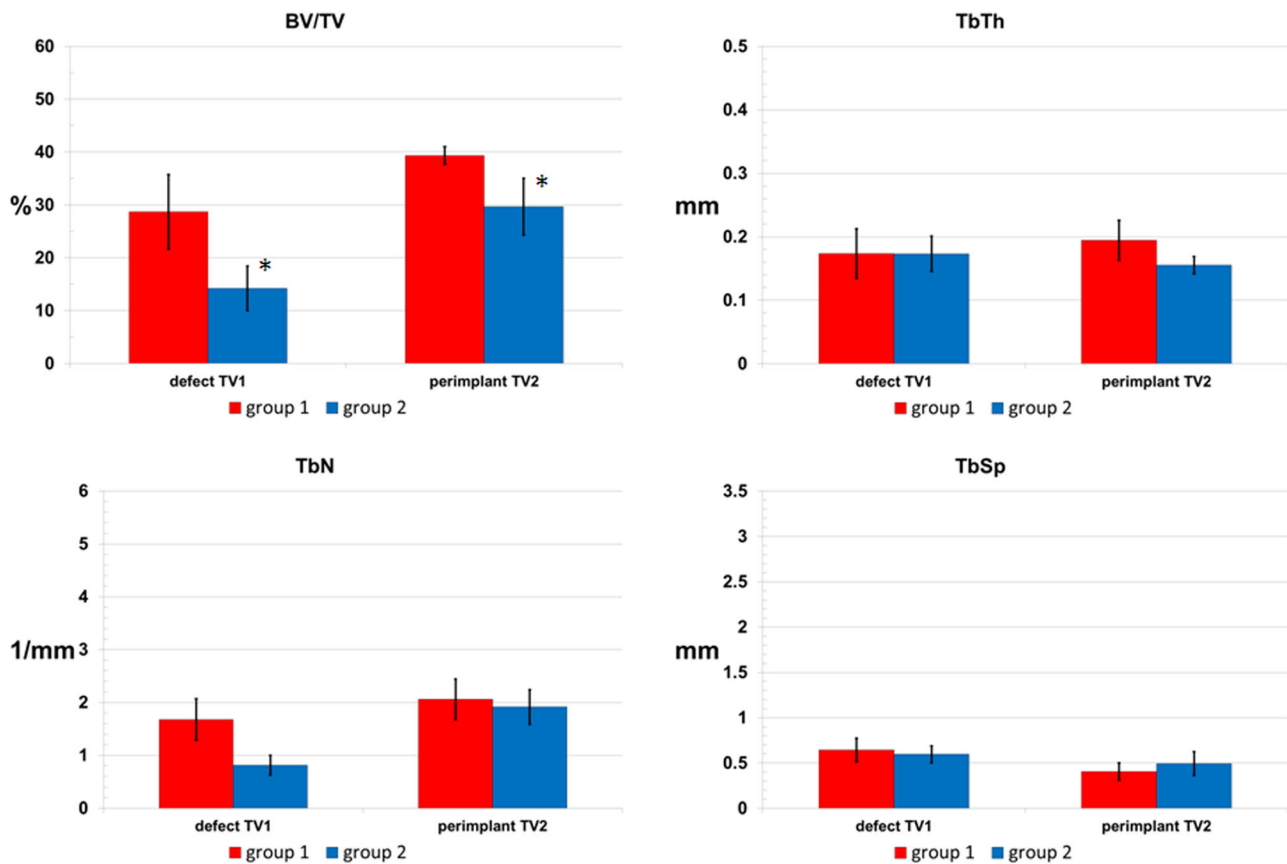


Fig. 2 Results of calculated 3D parameters relevant to new formed bone inside the defect and perimplant bone inside TV2 on control (group 1) and experimental group (group 2), in the rabbit model

(Bethyl Laboratories, Inc, TX). Sample reaction was developed with 3,3-diaminobenzidine substrate and permanently mounted.

2.4 Statistical analysis

Statistical analysis was performed using the IBM SPSS Statistics v.21. Data are reported as mean \pm SD at a significance level of $p < 0.05$. After having verified normal distribution and homogeneity of variance, the non-parametric Kruskal Wallis test followed by U Mann-Whitney was used to analyze microtomographic and histomorphometric data.

3 Results

3.1 Sheep

3.1.1 Macroscopic evaluation

All animals tolerated surgery well and survived the post-surgical period. Gait was normal without severe limp, and the joints seemed stable.

The joint inspection showed the absence of joint inflammation, adhesions between the joint capsule, fat pad and collateral joint compartment. Gross evaluation of untreated group specimens showed no bone and cartilage defect healing in one sample, and incomplete bone defect filling and irregular bone-cartilage surface in the remaining ones. In the experimental group cartilage defect healing occurred in 7 samples while no cartilage was detected in only one sample. Concerning the bony compartment, newly formed repair bone tissue was seen in 4 examined samples. In 3 samples incomplete bone defect filling occurred and in 1 of these samples a small cyst was seen. In the remaining one sample no bone defect healing occurred. Evaluation of the macroscopic appearance with the modified Fortier score showed significant higher values in the experimental group ($p < 0.05$). No significant differences were found in Niederauer score (Table 1).

3.1.2 Microtomography

In the untreated defect group, newly formed bone was detected in the defect, especially at the subchondral cortical bone level and close to the defect surfaces. However, all samples in the untreated defect group showed an incomplete

Table 1 Macroscopic appearance of the implants and the quality of healing assessed using a modified scoring system from Fortier (max 0–min 15) and a scoring system proposed by Niederauer (max 8–min 0)

Group	Scoring system used for the gross appearance modified by Fortier et al.		Scoring system for the gross morphological evaluation modified by Niederauer et al.	
	CFM 15 min < 0 max	CFL 15 min < 0 max	CFM 0 min < 8 max	CFL 0 min < 8 max
Control	5.50 ± 2.12	8 ± 2.83	3 ± 1.41	3 ± 1.41
Experimental group	9.75 ± 1.71	9.25 ± 1.71	3.75 ± 0.50	3.50 ± 0.58

Data were reported as mean ± standard deviation (SD)

T-test analysis: * $p < 0.05$

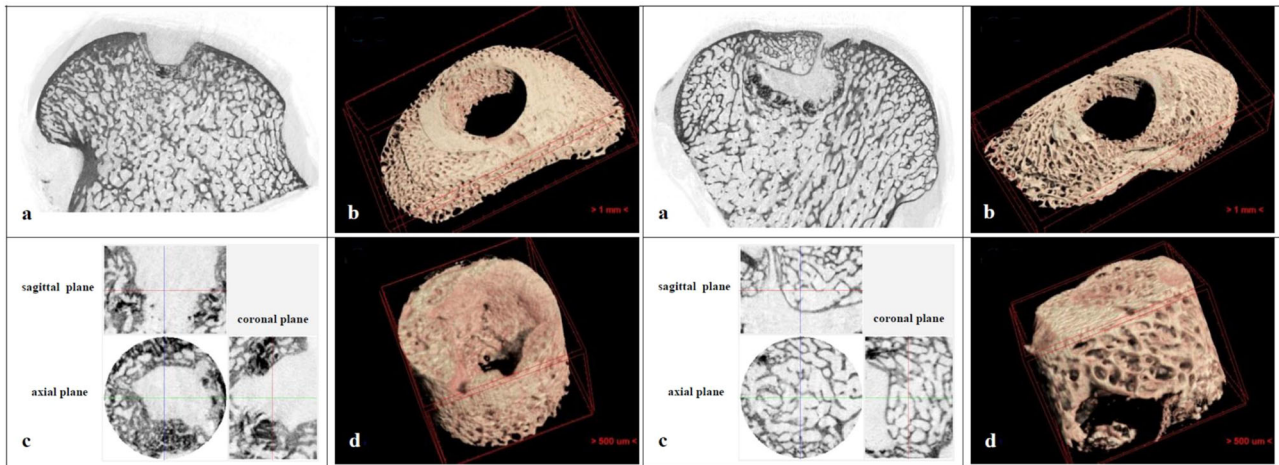


Fig. 3 Micro-CT sections and 3D models of samples in study group—Alginate-based biphasic scaffold, in the sheep model. Each panel is organized as follows: **a** Sagittal Micro-CT section of the condyle; **b** 3D

model of perimplant trabecular bone in TV2; **c** Micro-CT sections in the three spatial planes (axial, sagittal and coronal) of TV1; **d** 3D model of the newly formed bone into TV1

healing, especially at the center of the defect leading to a concave surface in the subchondral cortical bone. In the experimental group the newly formed bone was not present uniformly, leading to an incomplete bone regeneration inside the defect (Fig. 3).

3D morphometric analysis was performed, showing lower BV/TV and Tb.Th values, and higher Tb.N at peri-implant bone level (each: $p < 0.05$) in the experimental group compared to control (Fig. 4). On the other hand, 3D morphometric parameters analysis on bone inside the defect didn't show significant differences between experimental and control groups, principally due to a high intra-group variability.

The analysis was also conducted two-dimensionally, i.e. section by section, to evaluate the distribution of all bone parameters along the defect depth. The 2D distribution results on bone inside the defect and at peri-implant level, divided between medial and lateral condyle levels, did not show any significant difference.

3.1.3 Histology

Histological assessment confirmed the macroscopic results. In group 1, one sample showed no healing of bone and

cartilage at the defect site, which was filled instead with amorphous fibrous tissue. Incomplete bone filling and irregular bone-cartilage surface were observed in the remaining samples, where chondrocytes were grouped in clusters.

In group 2, newly formed cartilage tissue and good integration of the scaffolds with the host cartilage was observed in seven of the examined samples. In addition, Safranin O staining showed signs of proteoglycan synthesis in all these samples. Concerning the bony compartment, no interposition of connective tissue was observed in seven cases, being the scaffold in close contact with the surrounding trabecular bone tissue. In addition, newly formed bone tissue seeped into the scaffold and osteoid matrix consisting of osteoblast lining new trabeculae were detected both onto material porosities and onto the surface of bone trabeculae (Fig. 5). In three of these samples bone defect filling was still not complete and a small cyst was present in one case, filled with amorphous fibrous tissue. No bone and cartilage defect healing occurred in one case, where only fibrous tissue filled the defect.

The semiquantitative analysis performed with the Pineda score showed significantly better values in the experimental group compared to control (Table 2).

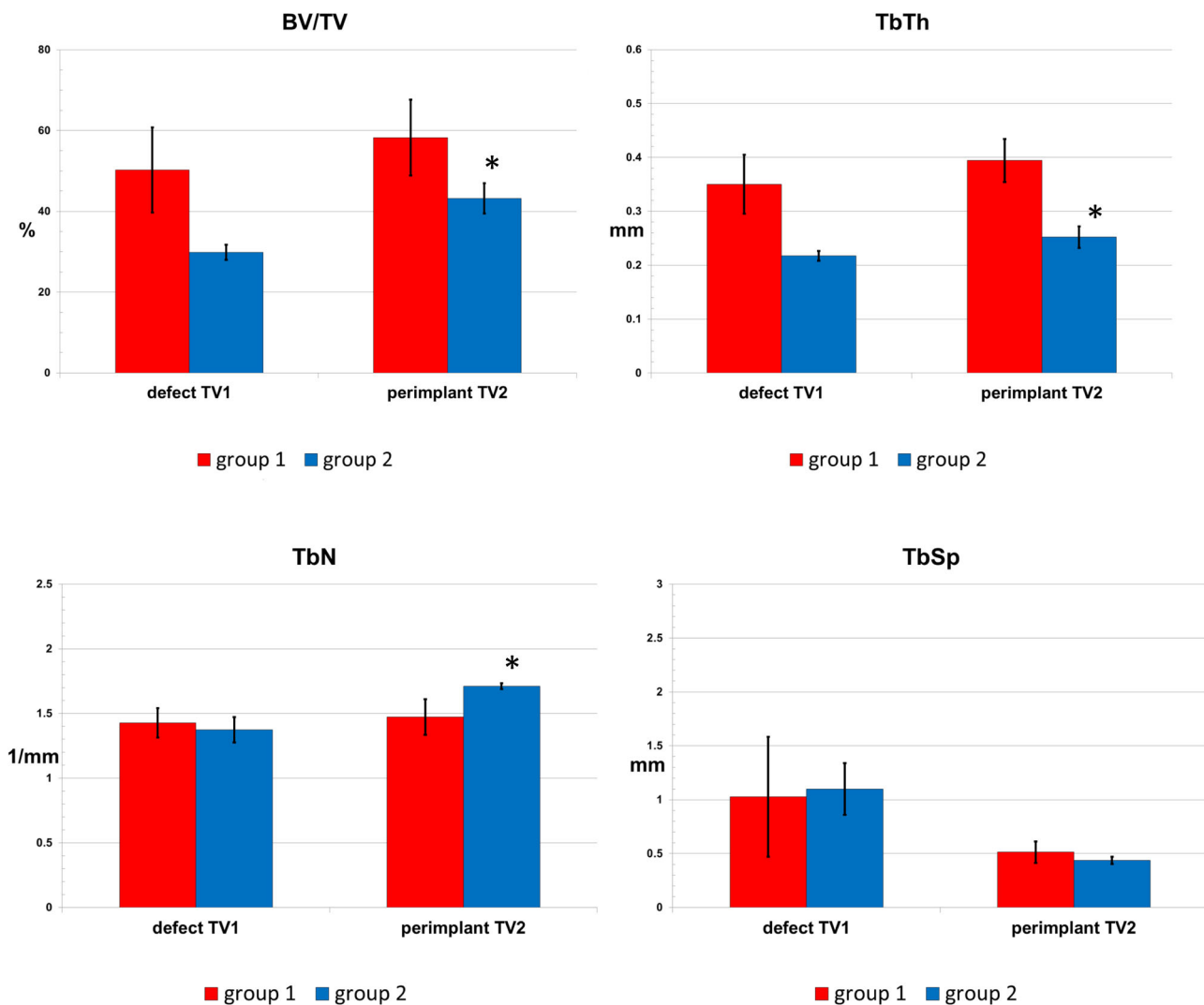


Fig. 4 Results of calculated 3D BV/TV, TbTh, TbN and TbSp parameters relevant to newly formed bone inside the defect and perimplant bone inside TV2 on control (group 1) and experimental group (group 2) (sheep model)

3.1.4 Immunohistochemistry

Type I and II collagen staining were either negative or positive in scattered areas of both groups, as visible in Fig. 6. In detail, in Untreated Group Type I Collagen staining was slightly hinted in the superficial cartilaginous layer while greater positivity was detected in all the other cartilaginous layers up to the subchondral bone. In the experimental group Type I Collagen staining was almost positive in all the cartilaginous layers with a more intense positivity in the deeper layer over the subchondral bone. Regarding Type II Collagen, the Untreated group showed a strongly positivity in the middle layers while a slightly positive was seen in the superficial and deep cartilaginous layers. Differently, in experimental group Type II Collagen was positive in scattered areas of all cartilaginous layers with a greater positivity detected in the middle

layers. Concerning VEGF immunohistochemical analysis, a positive staining in the cartilage extracellular matrix, extended throughout the repair tissue up to the joint space, was seen in both Groups with no significant differences.

3.2 Rabbits

3.2.1 Macroscopic evaluation

Anesthesia procedures and postoperative period were uneventful for all animals. Some peri-articular fibrotic tissues were detected macroscopically in 1 case for each group. Three of the 12 samples, both in the control and in the experimental groups presented an altered scaffold position, not fully surrounded by trabecular bone, and were therefore excluded from the analysis.

Fig. 5 Histological evaluations at 6 months of Group 2, Alginate-based biphasic scaffold. **a** Safranin-O/Fast green stain. Magnification 1×. **b** Magnification 10× and **c** 20×. **d** Haematoxylin/Eosin staining. Magnification 10× (sheep model)

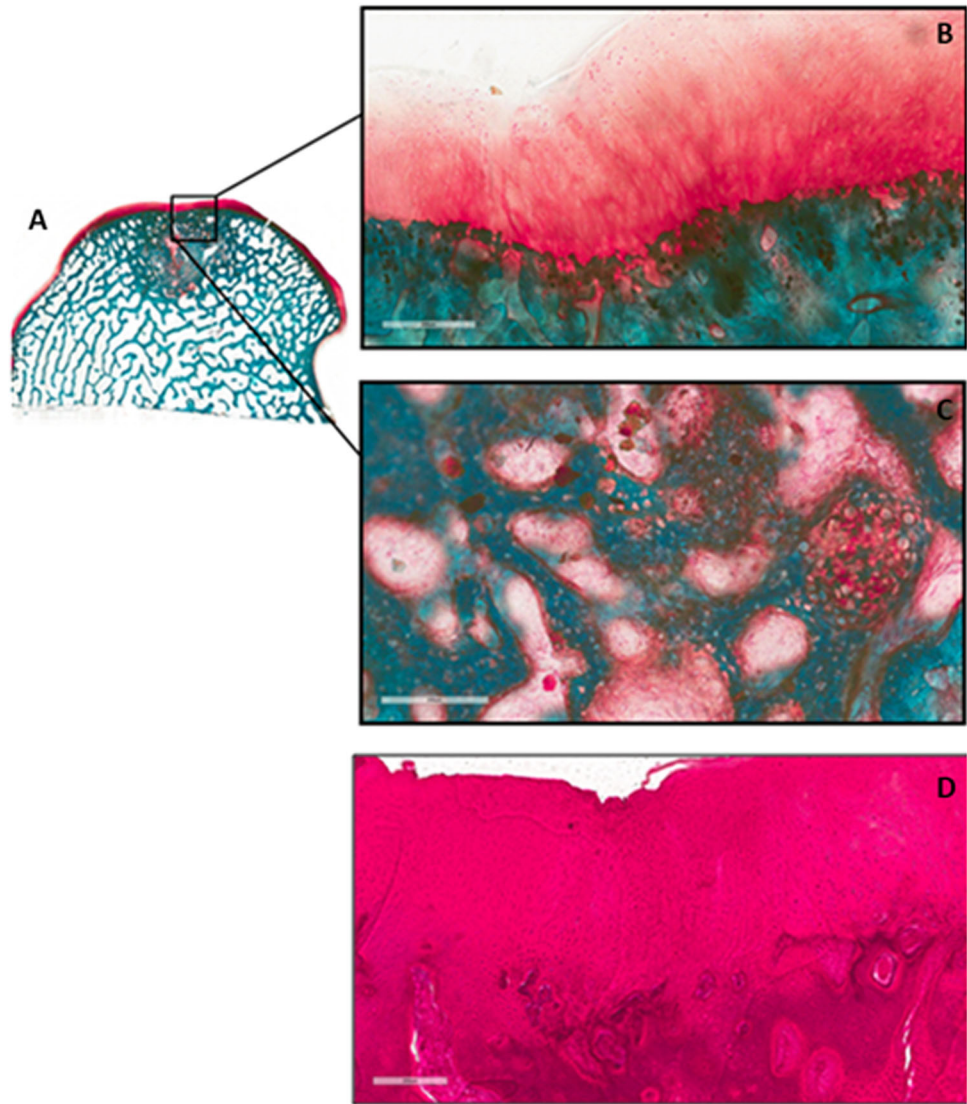


Table 2 Comparative histology evaluation rated using the Pineda score (Pineda et al. [24])

	Control	Mineralized alginate	<i>P</i> -value
Filling of the defect	3.00	1.75	<0.05
Reconstruction of osteochondral Junction	1.00	0.63	<0.05
Matrix staining	2.25	1.25	<0.05
Cell morphology	2.50	2.38	n.s.
Total	8.75	6.00	<0.05

3.2.2 Microtomography evaluation

The comparative analysis showed a lower formation of new bone inside the defect in group 2, with a lower BV/TV value both inside the defect ($p < 0.05$) and in the peri-implant area ($p < 0.05$) (Figs. 1, 2).

3.2.3 Histology and histomorphometry

In group 1, scaffold residuals were visible in 3/9 cases, surrounded by connective tissue. An intense bone tissue activity was observed around the connective tissue; this was characterized by woven bone matrix containing numerous densely packed and spherical osteocytes entrapped within new trabeculae and the osteoid matrix deposited by osteoblast lining new trabeculae. Scaffold resorption was observed in 6/9 cases, where new bone tissue filled the area originally occupied by the material. Finally, an inflammatory infiltrate was observed in 2/9 samples.

In group 2, the scaffold material was still well recognizable in all cases, even if its structural integrity was preserved only in 3/9, while signs of reabsorption were evident in 6/9 with internal vacuolization and fragmentation. In all cases a direct contact between the scaffold and the surrounding trabecular bone tissue was observed with no

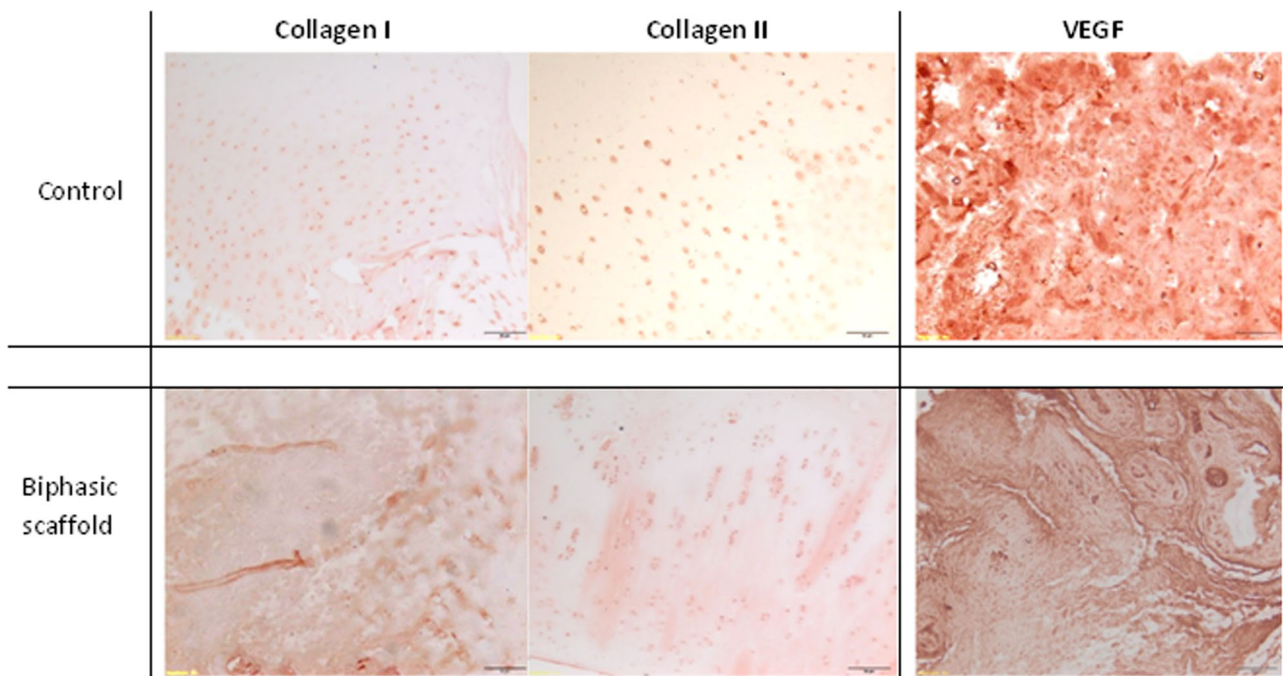


Fig. 6 Representative fields of immunohistochemical staining for type I, type II collagen and VEGF of decalcified samples at 6 months in group 1 and group 2. Magnification 10× (sheep model)

interposition of fibrotic or inflammatory tissue. The newly formed bone was always in close contact with the material, penetrating it where fissures were present. Osteoblasts and new bone tissue colonizing the scaffold were detected both onto material porosities and onto the surface of bone trabeculae. No fibrous tissue or inflammatory infiltrates were detected in all examined cases in this group (Fig. 7). All findings are summarized in Table 3.

Finally, statistical analysis revealed no significant differences between Group 1 and Group 2 for the dynamic histomorphometric parameters (MAR and BFR), as reported in Table 4.

4 Discussion

The main finding of this pilot preclinical study is that this mineralized alginate-based material presents a high biocompatibility, making it attractive for future applications, but currently this bioengineered strategy also presents limited bone regenerative properties, as shown by these animal models underlying the need for further developments to make it a feasible solution to support osteochondral regeneration.

The regeneration of an osteochondral defect is challenging, and the sheep model helped in evaluating *in vivo* the potential of this biomaterial. In fact, this large-size animal model represents a clinically-relevant benchmark due to the

loading conditions, with a comparable limb-loading between sheep and humans [27]. Moreover, pre-clinical tests in large animals allow the adoption of a surgical technique closely resembling that to be used in humans [28, 29]. In fact, it is generally agreed that the results obtained in large animals can satisfactorily represent the final target, then they are more useful for translational purposes, and in this setting this biphasic biomaterial showed promising but yet suboptimal findings for the development of a bioengineered strategy for osteochondral regeneration [15]. The limitations emerged regarding the potential of this osteochondral scaffold were further investigated in a less demanding medium-size animal model, which allowed to isolate the bone phase from the chondral one, without possible interferences from the intra-articular environment. In this setting, the ability of the mineralized alginate alone to regenerate bone tissue was compared to a commercially available product for bone regeneration. The rabbit model has previously been shown to be a suitable option for testing different biomaterials with regard to bone growth and repair [23]. The evaluation performed in this model confirmed a high biocompatibility profile, which was even higher than that of a commercially available product, but at the same time limited resorption and subsequent slow bone formation.

The biphasic material used in this study was developed [30] through a diffusion-controlled, directed ionotropic gelation of alginate leading to a monolithic, highly porous,

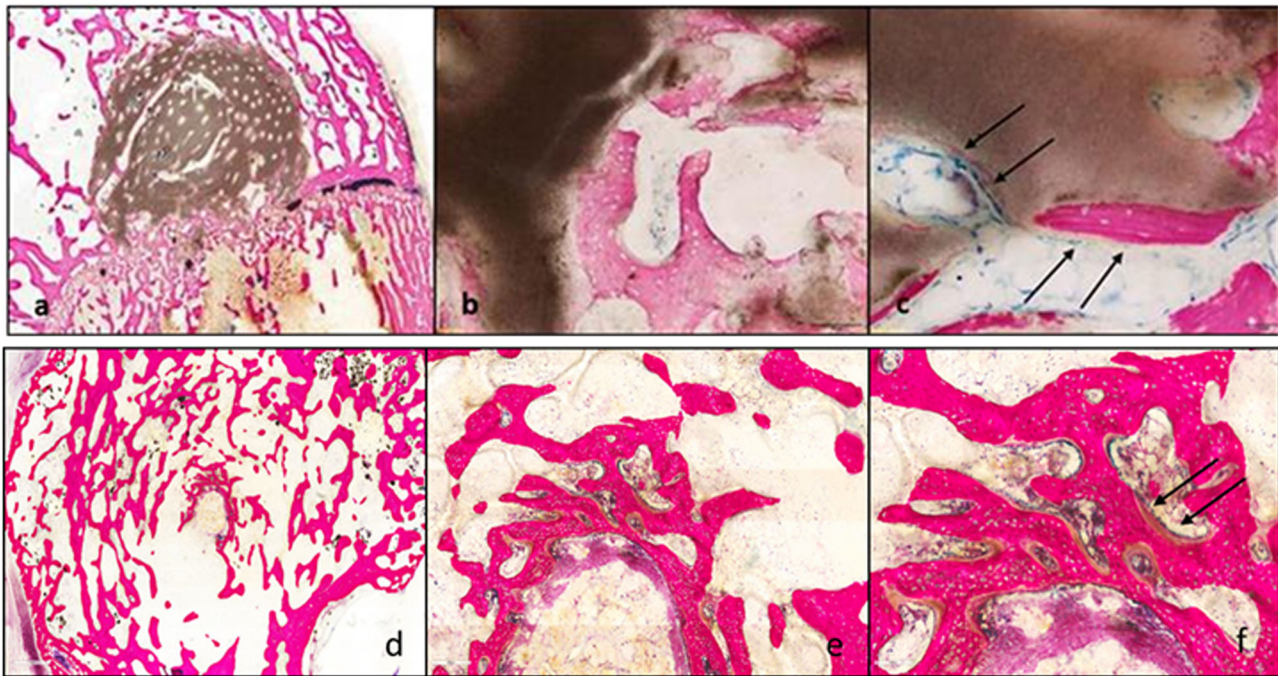


Fig. 7 Histologic evaluation of in the rabbit model at different magnifications and stained with Stevenel blue counterstained with van Gieson Pichrofucsin. Top: Mineralized Alginate. **a** magnification 2×; **b** magnification 10×; **c** magnification 40×: arrows highlight the osteoblast activity detected both onto material porosities than onto bone

trabeculae surface. Bottom: Control group. **d** magnification 2×; **e** magnification 10×; **f** magnification 40×: arrows highlighted the osteoblast lining new trabeculae actively involved in osteoid matrix deposition

Table 3 Histological features observed at 2 months from surgery for each experimental and control group

		Group 1	Group 2
Defect area	Recognizable/Unchanged	1/9	3/9
	Recognizable/Reduced	8/9	6/9
	Repaired		
Material	Not even recognizable		
	Present/Evident		9/9
	Residuals	3/9	
Bone/Material contact	Fragmented		
	Not even recognizable	6/9	
	Present		9/9
Connective tissue	Partial		
	Absent		
	Present/Continuos	2/9	
Inflammatory infiltrate	Partially Present	1/9	
	Absent	6/9	9/9
	Present		
Not assessable	Slight	2/9	
	Absent	7/9	9/9
		3	3

anisotropic structure that resembles those of the bone tissue, aimed at facilitating blood vessel ingrowth and migration of the cells from the bone marrow. Previous in vitro studies

Table 4 Dynamic histomorphometric results related to oxytetracycline incorporation into newly calcifying bone grew inside or around experimental group (mineralized alginate scaffold) in comparison to control (RegenOss) material

	MAR	BFR
Group 1	0.89 ± 0.15	0.53 ± 0.18
Group 2	0.83 ± 0.19	0.69 ± 0.26
<i>p</i> -value	0.557	0.244

have shown that a similar alginate-HA scaffold promoted proliferation and osteogenic differentiation of human bone marrow stromal cells, with a high proliferation rate and an active expression of bone-related genes [31]. Finally, a further in vitro study showed that chondrogenically induced human MSCs embedded within the chondral layer of the biphasic scaffold used in this study differentiated into chondrogenic lineage [20].

Based on the positive in vitro evidence, we aimed at investigating in vivo this biomaterial in terms of biocompatibility and osteochondral regenerative potential.

The results of this study showed a good biocompatibility profile, with no evidence of adverse reactions nor the presence of inflammatory tissues surrounding the implants observed in both animal models. Macroscopic healing of

the cartilage defect was documented in most samples of the osteochondral sheep study, and the positive findings in terms of repair and implant integration of the cartilage layer were confirmed at histologic and histomorphometric analysis, even though presence of fibrocartilaginous tissue was also shown. More critical appeared the bone layer, showing abnormal filling in half of the cases; both qualitative and quantitative micro-CT evaluations showed incomplete bone tissue regeneration. This can be explained by the slow resorption rate already observed for the bone phase in the smaller model. In particular, in the bone study, fibrotic peri-articular tissue was found in one specimen (similarly to the findings observed with the commercially available product), but no inflammatory cell infiltrates were detected, no foreign body reaction could be documented and the construct did not elicit any adverse immunological rejection. However, the quantitative analysis on bone 3D morphometric parameters showed a lower formation of new bone in the experimental group. This minor formation must be analyzed by comparing the values of the morphometric parameters within the defect with the corresponding values of peri-implant bone in the two different models. Sheep model showed a comparable bone regeneration between control (untreated) and alginate scaffold (equal values of Tb.N). Therefore, the lower value of BV/TV1 may be advocated to the thickness of the bone trabeculae. A similar trend was found in the peri-implant bone as well in the same model. However, the amount of bone regeneration within the defect showed lower Tb.N in the rabbit model compared to control. This value is index of new bone formation, thus it is deducible that the alginate scaffold produced less bone regeneration compared to the commercially available scaffold. In addition, the lower BV/TV 2 value of the peri-implant bone was due both to decreased number and thickness of the bone trabeculae. After a normalization data within the defect with peri-implant bone, bone formation inside the defect in the presence of alginate showed comparable values to those of the untreated group. Also, the histomorphometric analysis showed comparable bone deposition rate in the experimental and control group in the sheep model. However, when compared to the commercial scaffold bone formation inside the defect was lower instead, with alginate material always recognizable into the defect area. Thus, the slow resorption time might explain the lower presence of newly formed bone into the defect.

Nonetheless, direct contact between the scaffold and the surrounding trabecular bone was observed, with evidence of scaffold colonization and new bone formation penetrating the fissures of the biomaterial. Finally, in addition to a possible inter-animal variability, the differences found for the peri-implant bone in both the animal models in the alginate group could be due

hypothesized in a sort of recall action made by the alginate anionic complexes to the mineral cations of inorganic bone matrix.

To this regard, the slow biodegradability of the hydrogel structure is not surprising [32], since non-tissue-derived materials already showed a poor biodegradability [12]. However, compared to other gel materials, alginate can dissolve into monomer subunits in presence of chelating agents, such as citrate [33], and this property might facilitate the subsequent removal of the alginate component [34]. Future studies should evaluate if the scaffold structure persists at longer follow-up and if any method is applicable to improve the resorption of the biomaterial. However, signs of reabsorption processes were already present, thus suggesting that the persistence of the scaffold is temporary, exerting in the early post-implant phase structural properties to favor load bearing while allowing cells to induce new extracellular matrix deposition. Moreover, the scaffold degradation may be enhanced, and consequently the possibility to have more bone substitution, by the use of the scaffold in a bioengineering strategy. In fact, *in vitro* studies showed a promising behavior of precursor cells seeded into the biomaterial, and the implantation of cellularized grafts might be beneficial in terms of better tissue regeneration, as BMSCs augmentation may enhance the regenerative properties of different biomaterials [35].

Even though some aspects have to be further explored in terms of both improvement of material properties and scaffold-cell interaction, bio-inspired scaffold fabrication based on alginate showed to be a suitable, relatively low-cost method to obtain biocompatible biphasic osteochondral scaffolds. The study findings pave the way for the use of this monolithic alginate-based material as scaffold to develop a bioengineered strategy to restore the articular surface.

In conclusion, this biphasic alginate scaffold comprising a mineralized bony part and a non-mineralized chondral part showed a good biocompatibility profile, both for segmental bone and osteochondral regeneration, as shown by this *in vivo* investigation. Modest bone substitution of the scaffold was observed in the sheep model, with slow resorption time. Further investigation by comparison with a commercially available product for bone regeneration in the rabbit model, showed lower bone formation and still recognizable scaffold residuals due to the longer persistence of the biomaterial, but lower inflammatory induction as well compared to control. Further studies are needed to investigate if the promising findings documented in this study supporting the use of this alginate-based scaffold for a bioengineering approach can be confirmed and optimized, identifying the optimal biological augmentation strategy to further enhance the potential of this biomaterial for osteochondral regeneration.

Acknowledgements This study was supported by European Project OPHIS-COMPOSITE PHENOTYPIC TRIGGERS FOR BONE AND CARTILAGE REPAIR (FP7-NMP-2009-SMALL 3-246373).

Author contributions GF: conception and design of the study, animal surgery, manuscript drafting. FP: collaboration for animal surgery, macroscopic evaluations, manuscript drafting. MG: scaffold development and production, manuscript drafting. MF: manuscript drafting, analysis and interpretation of the data, final approval of the article. FD: scaffold development and production, manuscript drafting. MM: senior scientific consultant, critical revision of the article. APP: microtomography analysis. AR: logistic support, assembly of the data, manuscript drafting. FS: histological and histomorphometric analysis on sheep. MS: histological analysis on rabbits. KS: scaffold development and production, manuscript drafting. EK: obtaining of funding, conception and design of the study, animal surgery, final approval of the article

Compliance with ethical standards

Conflict of interest GF is consultant for: Finceramica Faenza S.p.A, Italy; Fidia farmaceutica, Italy; CartiHeal ltd (2009) Israel, EON Medica, Italy. MM receives royalties from Finceramica Faenza S.p.A., Italy. EK is consultant for Finceramica Faenza S.p.A., Italy; CartiHeal (2009) ltd, Israel. GF, EK, MM receive Institutional Support from FinCeramica Faenza S.p.A.; Fidia farmaceutica, Italy, IGEA Biomedical, Italy, Zimmer-BIOMET, USA, Kensey Nash, USA. The remaining authors declare that they have no conflict of interest.

References

- Gomoll AH, Filardo G, de Girolamo L, et al. Surgical treatment for early osteoarthritis. Part I: cartilage repair procedures. *Knee Surg Sports Traumatol Arthrosc.* 2012;20:450–66.
- Gomoll AH, Filardo G, Almqvist FK, et al. Surgical treatment for early osteoarthritis. Part II: allografts and concurrent procedures. *Knee Surg Sports Traumatol Arthrosc.* 2012;20:468–86.
- Filardo G, Kon E, Di Martino A, et al. Is the clinical outcome after cartilage treatment affected by subchondral bone edema? *Knee Surg Sports Traumatol Arthrosc.* 2014;22:1337–44.
- Kon E, Roffi A, Filardo G, et al. Scaffold-based cartilage treatments: with or without cells? A systematic review of preclinical and clinical evidence. *Arthroscopy.* 2015;31:767–75.
- Abarrategi A, Lópiz-Morales Y, Ramos V, et al. Chitosan scaffolds for osteochondral tissue regeneration. *J Biomed Mater Res A.* 2010;95:1132–41.
- Amadori S, Torricelli P, Panzavolta S, et al. Multi-layered scaffolds for osteochondral tissue engineering: in vitro response of co-cultured human mesenchymal stem cells. *Macromol Biosci.* 2015;15:1535–45.
- Tampieri A, Sandri M, Landi E, et al. Design of graded biomimetic osteochondral composite scaffolds. *Biomaterials.* 2008;29:3539–46.
- Filardo G, Kon E, Perdisa F, et al. Osteochondral scaffold reconstruction for complex knee lesions: a comparative evaluation. *Knee.* 2013;20:570.
- Marcacci M, Zaffagnini S, Kon E, et al. Unicompartmental osteoarthritis: an integrated biomechanical and biological approach as alternative to metal resurfacing. *Knee Surg Sports Traumatol Arthrosc.* 2013;21:2509–17.
- Kon E, Filardo G, Di Martino A, et al. Clinical results and MRI evolution of a nano-composite multilayered biomaterial for osteochondral regeneration at 5 years. *Am J Sports Med.* 2014;42:158–65.
- Häuselmann HJ, Masuda K, Hunziker EB, et al. Adult human chondrocytes cultured in alginate form a matrix similar to native human articular cartilage. *Am J Physiol.* 1996;71:C742–52.
- Miralles G, Baudoin R, Dumas D, et al. Sodium alginate sponges with or without sodium hyaluronate: in vitro engineering of cartilage. *J Biomed Mater Res.* 2001;57:268–78.
- Park Y, Sugimoto M, Watrin A, et al. BMP-2 induces the expression of chondrocyte-specific genes in bovine synovium-derived progenitor cells cultured in three-dimensional alginate hydrogel. *Osteoarthr Cartil.* 2005;13:527–36.
- Genes NG, Rowley JA, Mooney DJ, et al. Effect of substrate mechanics on chondrocyte adhesion to modified alginate surfaces. *Arch Biochem Biophys.* 2004;422:161–67.
- Ma K, Titan AL, Stafford M, et al. Variations in chondrogenesis of human bone marrow-derived mesenchymal stem cells in fibrin/alginate blended hydrogels. *Acta Biomater.* 2012;8:3754–64.
- Guo JF, Jourdain GW, MacCallum DK. Culture and growth characteristics of chondrocytes encapsulated in alginate beads. *Connect Tissue Res.* 1989;19:277–97.
- Diduch DR, Jordan LC, Mierisch CM, et al. Marrow stromal cells embedded in alginate for repair of osteochondral defects. *Arthroscopy.* 2000;16:571–77.
- Ko HF, Sfeir C, Kumta PN. Novel synthesis strategies for natural polymer and composite biomaterials as potential scaffolds for tissue engineering. *Philos Trans A Math Phys Eng Sci.* 2010;368:1981–97.
- Kumar A, Akkineni AR, Basu B, et al. Three-dimensional plotted hydroxyapatite scaffolds with predefined architecture: comparison of stabilization by alginate cross-linking versus sintering. *J Biomater Appl.* 2016;30:1168–81.
- Schütz K, Despong F, Lode A, Gelinsky M. Cell-laden biphasic scaffolds with anisotropic structure for the regeneration of osteochondral tissue. *J Tissue Eng Regen Med.* 2016;10:404–17.
- Fortier LA, Mohammed HO, Lust G, Nixon AJ. Insulin-like growth factor-I enhances cell-based repair of articular cartilage. *J Bone Jt Surg Br.* 2002;84:276–88.
- Niederauer GG, Slivka MA, Leatherbury NC, et al. Evaluation of multiphase implants for repair of focal osteochondral defects in goats. *Biomaterials.* 2000;21:2561–74.
- Paul K, Lee BY, Abueva C, et al. In vivo evaluation of injectable calcium phosphate cement composed of Zn and Si-incorporated β -tricalcium phosphate and monocalcium phosphate monohydrate for a critical sized defect of the rabbit femoral condyle. *J Biomed Mater Res B Appl Biomater.* 2015. <https://doi.org/10.1002/jbm.b.33537>
- Pineda S, Pollack A, Stevenson S, et al. A semiquantitative scale for histologic grading of articular cartilage repair. *Acta Anat.* 1992;143:335–40.
- Venkatesan J, Kim SK. Chitosan composites for bone tissue engineering—an overview. *Drugs.* 2010;8:2252–66.
- Hoemann C, Hurtig M, Rossomacha E, et al. Chitosan glycerol phosphate/blood implants improve hyaline cartilage repair in ovine microfracture defects. *J Bone Jt Surg Am.* 2005;87:2671–86.
- Martini L, Fini M, Giavaresi G, Giardino R. Sheep model in orthopedic research: a literature review. *Comp Med.* 2001;51:292–99.
- Brehm W, Aklin B, Yamashita T, et al. Repair of superficial osteochondral defects with an autologous scaffold-free cartilage construct in a caprine model: implantation method and short-term results. *Osteoarthr Cartil.* 2006;14:1214.
- Buma P, Schreurs W, Verdonchot N. Skeletal tissue engineering—from in vitro studies to large animal models. *Biomaterials.* 2004;25:1487–95.

30. Gelinsky M, Eckert M, and Despong F. Biphasic, but monolithic scaffolds for the therapy of osteochondral defects. *Int JMater Res.* 2007;98:749–55.
31. Bernhardt A, Despong F, Lode A, et al. Proliferation and osteogenic differentiation of human bone marrow stromal cells on alginate-gelatine-hydroxyapatite scaffolds with anisotropic pore structure. *J Tissue Eng Regen Med.* 2009;3:54–62.
32. Park H, Lee KY. Cartilage regeneration using biodegradable oxidized alginate/hyaluronate hydrogels. *J Biomed Mater Res A.* 2014;102:4519–25.
33. Leddy HA, Awad HA, Guilak F. Molecular diffusion in tissue-engineered cartilage constructs: effects of scaffold material, time, and culture conditions. *J Biomed Mater Res B Appl Biomater.* 2004;70:397–406.
34. Perka C, Spitzer RS, Lindenhayn K, et al. Matrix-mixed culture: new methodology for chondrocyte culture and preparation of cartilage transplants. *J Biomed Mater Res.* 2000;49:305–11.
35. Filardo G, Perdisa F, Roffi A, et al. Stem cells in articular cartilage regeneration. *J Orthop Surg Res.* 2016;11:42.